Applied Surface Science 567 (2021) 150901

Contents lists available at ScienceDirect

Applied Surface Science

journal homepage: www.elsevier.com/locate/apsusc

Full Length Article

Surface free energy and wettability properties of transparent conducting oxide-based films with Ag interlayer

Salih Ozbay [a,*], Nursev Erdogan [b], Fuat Erden [c], Merve Ekmekcioglu [d,e], Busra Rakop [b], Mehtap Ozdemir [d], Gulnur Aygun [e], Lutfi Ozyuzer [d,e]

[a] Department of Chemical Engineering, Sivas University of Science and Technology, 58000 Sivas, Turkey
[b] Advanced Material, Process and Energy Technology Center, Turkish Aerospace, 06980 Ankara, Turkey
[c] Department of Aeronautical Engineering, Sivas University of Science and Technology, 58000 Sivas, Turkey
[d] Teknoma Technological Materials Inc., Izmir Technology Development Zone, Urla 35430, Izmir, Turkey
[e] Department of Physics, Izmir Institute of Technology, Urla 35430, Izmir, Turkey

ARTICLE INFO

Keywords:
Indium tin oxide
Aluminum zinc oxide
Zinc tin oxide
Silver
Surface free energy
Work of adhesion

ABSTRACT

ITO, ZTO, AZO and Ag are commonly used in transparent conducting oxide (TCO)/metal/TCO electrodes to form multilayered thin films on a suitable substrate. A detailed surface free energy (SFE) knowledge of these films is critical to design desirable TCO-based sandwich structures. In this study, TCO/Ag/TCO multilayer thin films were coated onto glass substrates using ITO, ZTO, AZO and Ag targets by magnetron sputtering. The wettability properties of TCO, Ag interlayer and TCO/Ag/TCO were evaluated by contact angle measurements of seven different liquids having various surface tension values. The dispersive and polar components of SFE were calculated using geometric and harmonic mean approaches. The acidic and basic components of SFE were calculated using van Oss-Chaudhury-Good method. Following this, the work of adhesion values between TCO films and Ag interlayer were estimated using SFE values of the films. The results show that the SFE components of the surfaces differ depending on the TCO type, the total SFE values of TCO/Ag/TCO films were lower than that of TCO films, and AZO/Ag adhesion is stronger than the other TCO/Ag structures. The reasons behind these differences were discussed by evaluating the SFE, XRD, AFM and SEM analysis simultaneously.

1. Introduction

Transparent conducting oxide (TCO) films play a key role in many technologically demanding applications because of their high optical transparency in the visible region and promising electrical conductivity [1]. However, a single layer of TCO films is often far from to meet the desired level of electrical conductivity, and the incorporation of a thin metal film between TCO layers without deteriorating the optical transparency is one of the options used to overcome this problem [2]. Ag is the most widely used interlayer material among metals due to its low electrical resistivity and suitability for magnetron sputtering systems [2–7]. Thus, the preparation of TCO/Ag/TCO multilayer films is a hot topic, and the physical properties of these sandwich films have been extensively studied previously for use in many applications such as organic light emitting diodes [8], ultraviolet light emitting diodes [9], electrochromic devices [10], organic solar cells [11], photovoltaic-thermoelectric hybrid systems [12] and flexible electronics [13].

In addition to optical and electrical properties, analysis of TCO-based films by means of surface thermodynamics approaches is also critical to produce a successful film [14]. In this context, controlling the surface properties such as wettability and surface free energy (SFE) of the interfaces of the designed structure within the desired range is crucial for adapting of TCO films to a specific application [15–37]. In many studies, the wettability properties of a TCO surface have been modified by applying plasma treatment methods such as O_2 plasma [16–21], H_2 plasma [19], air plasma [22,23], argon plasma [16,24,25], and Cl_2 plasma [26]. For example, You and Dong treated the ITO surface with O_2 plasma, and improved the interface formation and electrical contact of the ITO electrode with the organic compound by increasing the SFE of the ITO for use in organic light emitting diodes [18]. Vunnam et al. treated the ITO surface with air plasma to attain a favorable interface between printed nano-inks and ITO surface, and reported that the performance of printed electronic devices can be improved by controlling the SFE of the ITO [23]. Lee et al. treated the ITO surface with argon

* Corresponding author.
E-mail address: salihozbay@sivas.edu.tr (S. Ozbay).

https://doi.org/10.1016/j.apsusc.2021.150901
Received 8 June 2021; Received in revised form 20 July 2021; Accepted 6 August 2021
Available online 10 August 2021

atmospheric pressure plasma to increase the SFE of the ITO, and optimized the optical transmittance and sheet resistance of ITO glass by this way [25]. The wettability properties of a TCO surface can also be changed by using UV-ozone treatment [15,27,28]. To give an example, Dong et al. prepared sandwich type polymeric solar cells by coating an ITO interlayer treated with UV-ozone on top of an Ag reflector to increase the compatibility of interlayers by realizing a hydrophilic surface [28]. Apart from these, chemical treatment methods were also tried to control the surface properties of TCOs [29–31]. For instance, Besbes et al. treated the ITO surface by the use of self-assembled monolayer of an electron accepting phosphonic acid to increase the SFE of the ITO, and improved the ITO/polymer interface for using in organic light emitting devices [30]. Arazna et al. showed that the treatment of ITO surface in an ultrasonic bath of acetone and alcohol (ethyl alcohol or isopropyl alcohol) is effective for increasing the SFE of the ITO, and this modification might be useful in preparing ITO-based organic light emitting devices [31]. On the other hand, Saafi et al. showed that the controlling of the wettability characteristics of ZTO based films that can be used in gas and bio-sensors is critical for photocatalytic performance [37]. All of these studies clearly indicate that the wettability and SFE properties of TCO and TCO/metal/TCO have an important role in order to design a desired structure. Recently, we conducted a detailed SFE analysis in ITO/Au/ITO structures to clarify the effect of Au interlayer [14]. Our results showed that the total SFE values of ITO/Au/ITO multilayer thin films were higher than that of ITO surface. However, the effect of Ag interlayer on the SFE properties of TCO/Ag/TCO multilayer thin films still remained elusive.

Besides, there are many unanswered questions in this field to be considered regarding the adhesion relationships between interlayers. For example, how does the adhesion force between interlayers differ depending on the type of TCO and interlayer? Are there any force differences between top TCO and bottom TCO's adhesion to the interlayer? To the best of our knowledge, there is no paper focusing on these important cases. However, a detailed study on the adhesion properties of metal interlayer to the TCO films in such structures is getting more and more important as such systems are recently considered in flexible electronics. In order to answer these questions, the SFE components, which is critical to control many interface phenomena such as adhesion, adsorption, wetting, and lubrication behavior [38,39], of each interlayer must be determined most appropriately. As known, the determination of the SFE for solid surfaces cannot be done by direct methods due to the low mobility of solid molecules, and the SFE calculations based on contact angle measurements are probably the most efficient way that can be used for this purpose [40]. Yet, the SFE components of a surface might show deviations depending on many factors including the selection of liquid pairs used during calculations, and the method of SFE calculation [14,38–46]. Thus, it is often unfortunately impossible to obtain the correct SFE values for a solid surface without conducting a detailed examination.

The main aim of this study is to reach a detailed SFE knowledge of each interlayer in the TCO-based sandwich structures as accurately as possible by evaluating the wettability characteristics of TCO, Ag interlayer (TCO/Ag) and TCO/Ag/TCO multilayer thin films by SFE calculations. For this purpose, single layer of TCO, double layer of TCO (TCO/TCO), TCO/Ag and TCO/Ag/TCO films were deposited on soda lime glass (SLG) substrates by magnetron sputtering. The ITO, ZTO and AZO were selected as TCO materials in this study due to their popularity in the optoelectronic field. Seven different test liquids having various surface tension values were used to make more reliable evaluations, and the apparent contact angles of these liquids were measured on the prepared surfaces by the sessile drop method. Then, the dispersive and polar components of SFE were calculated using geometric (Owens and Wendt's method) [47] and harmonic (Wu's method) [48] mean approaches. The acidic and basic components of SFE were calculated using van Oss-Chaudhury-Good method [49]. According to the calculations, it was observed that the presence of Ag interlayer between the TCO layers had an important effect on the SFE properties of the sandwich films. In addition, the work of adhesion (W_a) values between TCOs and Ag interlayer were estimated using the calculated SFE values of each interlayer based on the Dupré, Fowkes and Girifalco-Good equations [50–55]. The results obtained by using surface thermodynamics approaches were also supported with various characterization methods such as XRD, AFM, and SEM.

2. Experimental section

2.1. Materials

AZO target was composed of ZnO (98 wt%) and Al_2O_3 (2 wt%), ITO target was composed of In_2O_3 (90 wt%) and SnO_2 (10 wt%), and ZTO target was Zn_2SnO_4. The dimensions of these TCO targets, as well as the high purity (99.99%) Ag target, were 2 in. diameter and 0.25 in. thickness. Soda lime glass (76 × 26 mm) was used as the substrate. Ultrapure water (CAS Number: 7732-18-5), methanol (CAS Number: 67-56-1), acetone (CAS Number: 67-64-1), formamide (CAS Number: 75-12-7), and diiodomethane (CAS Number: 75-11-6) were purchased from Merck. Glycerol (CAS Number: 56-81-5), ethylene glycol (CAS Number: 107-21-1), 1-bromonaphthalene (CAS Number: 90-11-9), and hexadecane (CAS Number: 544-76-3) were purchased from Sigma-Aldrich.

2.2. Preparation of TCO/Ag/TCO multilayer thin films on glass substrate

TCO and Ag thin films were deposited on SLG by direct current (DC) magnetron sputtering. Prior to deposition, the substrates were cleaned by ultrasonication in acetone, methanol and DI water for 10 min, respectively. Then, further cleaning was conducted by oxygen plasma etching for 2 min to eliminate organic residues. In a regular sputtering procedure, the chamber was first evacuated below 2×10^{-6} Torr. Following this, a pre-sputtering was conducted for 10 min to remove the contaminants. Finally, the deposition was carried out at about 2×10^{-3} Torr in Ar atmosphere at room temperature. The Ar flow rates were kept at 40 sccm during Ag deposition, and at 40, 30 and 30 sscm during ITO, ZTO and AZO depositions, respectively. The distance between all targets and the substrates was 7 cm. More details regarding the deposition parameters were given in Supplementary Material Table S1.

2.3. XRD, AFM, and SEM analysis

Grazing Incidence X-Ray Diffraction (GIXRD) was conducted by Panalytical X-Ray Diffractometer, with Cu-Kα radiation (λ = 1.5406 Å) and at a grazing angle of 0.75° between 2θ = 20-70° with a step size of 0.08° for all samples. The topographical features of the as-prepared films and the roughness values were determined by atomic force microscopy (AFM) in a tapping mode and under ambient conditions by using a silicon cantilever (SI-DF20, Seiko Instruments). The backscattered electron (BSE) images of cross sectional morphologies of the films were obtained using high resolution FEI NOVA Nanolab field emission scanning electron microscopy (FESEM) at an accelerating potential of 5 kV after milling of surface by focused ion beam (FIB) lithography. In order to protect the films, Pt was coated on the surface before ion etching. The thicknesses of the as-prepared films were measured by cross section SEM images and a Veeco Dektak 150 surface profilometer. The surface profilometer measurements were repeated from 3 different regions on the surface of all sandwich structures and the average thickness values of sandwich structures were 86.9 nm, 94.5 nm and 89.5 nm for AZO/Ag/AZO, ITO/Ag/ITO, and ZTO/Ag/ZTO, respectively.

2.4. Contact angle measurements

The apparent contact angles (θ) under air were determined by the sessile drop method using Biolin Scientific Attension Theta Lite contact

angle measurement system with a PC-controlled motorized syringe. 5 μL drops of water (W), glycerol (GLY), formamide (FA), diiodomethane (DM), ethylene glycol (EG), 1-bromonaphthalane (BN), and hexadecane (HD) were formed on the surfaces. Then, contact angles were determined after the needle was removed from the liquid droplet formed on the surface. Only the initial values, which were recorded within 1–2 s following the removal of the needle from the droplet, were reported as apparent contact angle. The contact angles were measured on at least five different places of each surface for all of the test liquids and the mean values were reported.

3. Results and discussion

3.1. Characterization, wettability properties and surface free energy analysis of TCO/Ag/TCO surfaces

The apparent contact angle results of the seven different test liquids on TCO-based surfaces are given in Table 1. The prepared surfaces were flat and gave repeatable contact angle results with a maximum deviation of ± 2°. In general, if θ_W is smaller than 90°, the surface is considered as hydrophilic, however if θ_W is larger than 90°, it means that the surface is hydrophobic [38,46]. The W contact angles were found to be larger than 90° for all tested TCO films, indicating that the as-prepared AZO, ITO and ZTO films on SLG substrates were led to formation of a hydrophobic surface. It was determined that W contact angle results of TCO films increase with the increase of their hydrophobicity in the following order: AZO ($\theta_W = 98°$) < ITO ($\theta_W = 102°$) < ZTO ($\theta_W = 104°$). Whereas, the W contact angle values for AZO/Ag/AZO, ITO/Ag/ITO, and ZTO/Ag/ZTO were found as 101°, 105°, and 105°, respectively. These results clearly indicate that the type of TCO and the presence of Ag interlayer between TCO layers have a significant influence on the wettability characteristics of the thin films formed. Surface properties of the TCO double coating (TCO/TCO) without Ag interlayer were also analyzed to make clarify the effect of the presence of Ag interlayer. The W contact angle values for AZO/AZO, ITO/ITO, and ZTO/ZTO were found as 94°, 102°, and 102°, respectively, indicating that water repellency of TCO/Ag/TCO surfaces is higher than both TCO and TCO/TCO films. In addition, similar W contact angle values on multilayered ITO and ZTO films, both with and without Ag interlayer, suggest that the effect of In and Zn to change the three-phase contact line of the water droplet is negligible. The oil repellency of the TCO surfaces were also evaluated by determining the contact angles of HD liquid, which is generally accepted as oleophobicity index [56]. The HD contact angle was measured as 25° for the ZTO/ZTO film, and 27° for the ZTO/Ag/ZTO film, all of which are comparable with the ITO-based films. However, the HD contact angle was found as 6° for the AZO/AZO film, and 20° for the AZO/Ag/AZO film, indicating that the AZO/HD interactions were stronger than the both ITO/HD and ZTO/HD interactions.

Table 1
Apparent contact angle (°) results on TCO, TCO/TCO, TCO/Ag, and TCO/Ag/TCO surfaces.

Surface	θ_W (°)	θ_{GLY} (°)	θ_{FA} (°)	θ_{DM} (°)	θ_{EG} (°)	θ_{BN} (°)	θ_{HD} (°)
AZO	98 ± 1	93 ± 1	80 ± 2	55 ± 2	73 ± 2	44 ± 2	7 ± 1
AZO/AZO	94 ± 2	90 ± 1	77 ± 1	51 ± 2	70 ± 2	40 ± 2	6 ± 1
AZO/Ag	108 ± 2	98 ± 1	89 ± 1	63 ± 2	83 ± 1	59 ± 1	25 ± 2
AZO/Ag/AZO	101 ± 2	94 ± 1	81 ± 2	59 ± 2	78 ± 1	53 ± 2	20 ± 1
ITO	102 ± 2	94 ± 1	87 ± 2	64 ± 1	77 ± 2	55 ± 1	22 ± 2
ITO/ITO	102 ± 2	93 ± 1	87 ± 2	63 ± 2	77 ± 2	53 ± 2	21 ± 2
ITO/Ag	107 ± 1	95 ± 1	90 ± 1	66 ± 1	81 ± 1	60 ± 1	27 ± 1
ITO/Ag/ITO	105 ± 1	95 ± 1	89 ± 1	65 ± 1	81 ± 1	58 ± 2	26 ± 1
ZTO	104 ± 1	94 ± 1	90 ± 1	66 ± 1	79 ± 1	58 ± 1	27 ± 1
ZTO/ZTO	102 ± 1	93 ± 1	86 ± 1	65 ± 1	76 ± 1	56 ± 1	25 ± 1
ZTO/Ag	109 ± 1	98 ± 1	91 ± 1	68 ± 2	84 ± 1	61 ± 1	28 ± 1
ZTO/Ag/ZTO	105 ± 1	95 ± 1	90 ± 1	67 ± 1	81 ± 1	59 ± 1	27 ± 2

W: Water, GLY: Glycerol, FA: Formamide, DM: Diiodomethane, EG: Ethylene glycol, BN: 1-Bromonaphthalene, HD: Hexadecane.

To evaluate the wettability properties of TCO films, let us consider the work of adhesion (W_a) values between various liquids having different surface tensions and TCO films. The W_a values were calculated by Young-Dupré equation [$W_a = \gamma_{LV}(1 + cos\theta)$] for all tested liquids [50], where γ_{LV} denotes surface tension values of the liquids used in this equation. The W_a values for W-AZO interface decreased sharply from 67.7 mJ/m^2 to 58.9 mJ/m^2 with the presence of Ag interlayer between AZO layers as given in Fig. 1(a). Similar trends were also observed for other tested liquids and other TCOs as given in Fig. 1(a) and Supplementary Material Fig. S1. These results suggest that Ag interlayer inserted between TCO layers in thin films could generate repulsive interactions with liquids which located over the outer layer. Regarding all TCOs including sandwich structures, ITO- and ZTO-based films gave similar W_a values, which were lower than AZO-based films. In addition, the W_a values for both DM-TCO and BN-TCO interfaces were quite higher than polar liquids-TCO interfaces as seen in Fig. 1(a) and (b). These results indicate that all TCOs have mainly dispersive surface character and the presence of Ag interlayer is effective for changing the liquid-TCO interactions. However, a detailed SFE analysis of TCO/Ag/TCO films is necessary to verify this statement.

The SFE components including Lifshitz-van der Waals and acid-base interaction parameters of the surfaces were calculated by applying acid-base (van Oss-Chaudhury-Good method) approach [49]. The main equation of the van Oss-Chaudhury-Good method can be written as,

$$\gamma_{LV}(1+\cos\theta) = 2\left(\sqrt{\gamma_S^{LW}\gamma_L^{LW}} + \sqrt{\gamma_S^{+}\gamma_L^{-}} + \sqrt{\gamma_S^{-}\gamma_L^{+}}\right) \quad (1)$$

where subscript S denotes solid, L liquid, V vapor, and γ_i^{LW} is the Lifshitz-van der Waals SFE term which comprises "dispersion (London)", "orientation (Keesom)" and "induction (Debye)" interactions [49,57]. The surface tension components of the liquids used in van Oss-Chaudhury-Good method were obtained from the literature [38,58–60], and given in Supplementary Material Table S2. Other equations are,

$$\gamma_i^{AB} = 2\sqrt{\gamma_i^{+}\gamma_i^{-}} \quad (2)$$

$$\gamma_i^{Tot} = \gamma_i^{LW} + \gamma_i^{AB} \quad (3)$$

where subscript i denotes liquid or solid, γ_i^+ denotes Lewis acid parameter, γ_i^- denotes Lewis base parameter, and γ_i^{AB} comprises all the electron donor–acceptor (acid-base) interactions that originate from the hydrogen bonding or π-electrons [40,49]. DM and BN were chosen as the nonpolar liquids, and W-FA, W-EG, W-GLY liquid pairs were selected as the polar liquids in evaluating the SFE components using the three-liquid acid-base method [49]. Because, the good compatibilities associated with the use of W-FA-DM/BN, W-EG-DM/BN, W-GLY-DM/BN liquid triples during calculations were already determined by Della Volpe et al. [44,45]. Accordingly, γ_S^{LW} was calculated by using θ results of DM and BN liquids, and then W-GLY, W-EG, W-FA θ pairs were used to calculate γ_S^+ and γ_S^- values [38,46,49].

The SFE results obtained for AZO-, ITO- and ZTO-based films by using these six different liquid combinations are given in Supplementary Material Table S3, S4 and S5, respectively. It is clearly seen that the van Oss-Chaudhury-Good method gives similar γ_S^{Tot} values for the same TCO

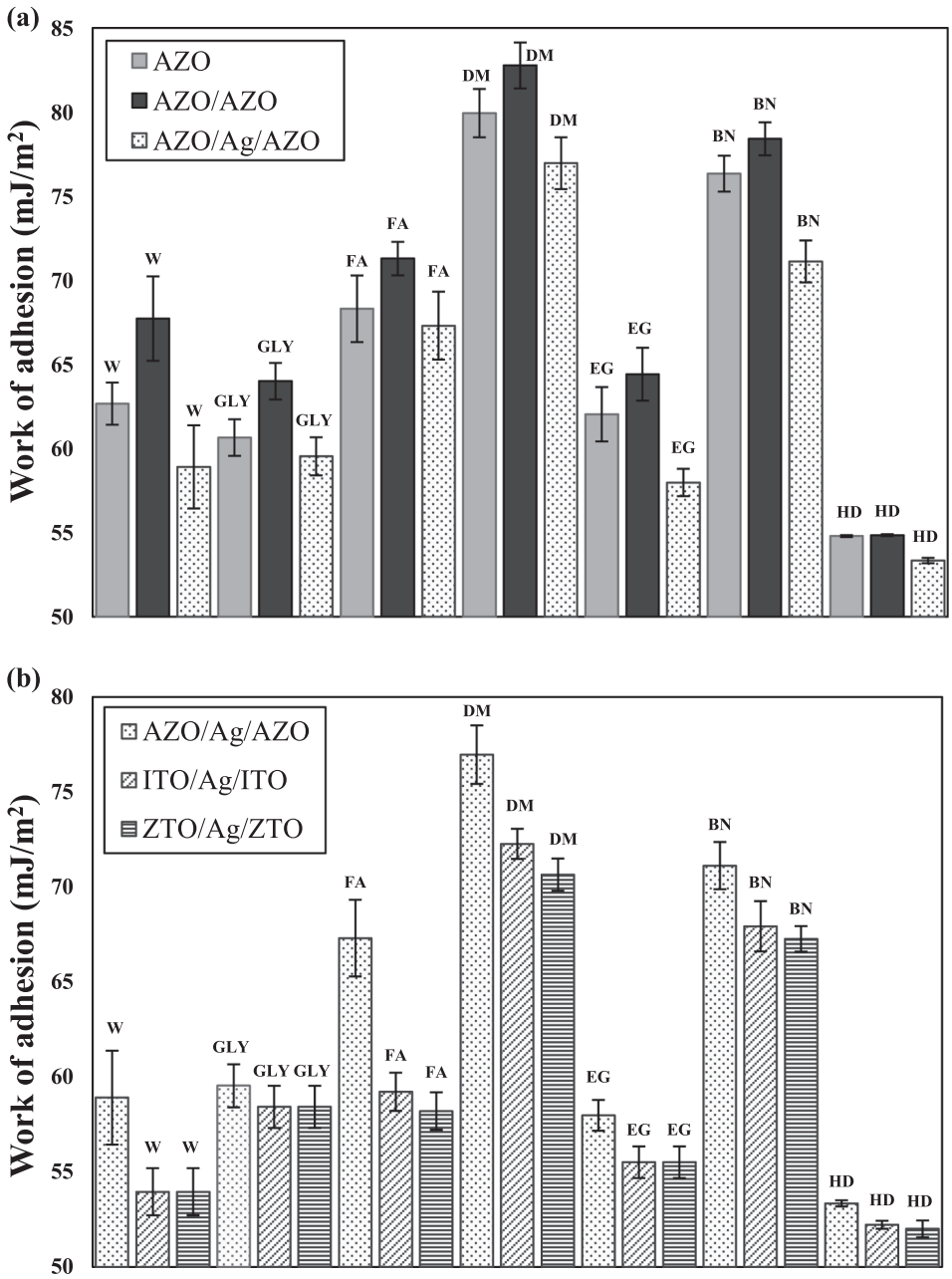

Fig. 1. Work of adhesion values of (a) AZO, AZO/AZO, AZO/Ag/AZO, (b) AZO/Ag/AZO, ITO/Ag/ITO, ZTO/Ag/ZTO surfaces. W, Water; GLY, glycerol; FA, formamide; DM, diiodomethane; EG, ethylene glycol; BN, 1-Bromonaphthalene; HD, hexadecane.

surface even if the liquid triple used is changed. For example, by using the W-FA-DM and W-GLY-DM liquid triples, the γ_S^{Tot} of ZTO/Ag/ZTO was found as 24.56 mJ/m^2, and this value was close to 25.48 mJ/m^2 which was found by using W-FA-BN, W-EG-BN and W-GLY-BN liquid triples. Similarly, the γ_S^{Tot} values for AZO/Ag/AZO, and ITO/Ag/ITO were calculated as 29.15, and 25.70 mJ/m^2, respectively using all liquid triples containing DM. On the other hand, the results of some SFE components might differ depending on the liquid pairs used. For example, the γ_S^- component of the SFE was found as 0.54 mJ/m^2 with W-EG-DM triple for ITO/Ag/ITO surface, indicating that the Lewis base parameter of the surface is very low. Whereas, the γ_S^- of the very same surface could also be calculated as 1.72 or 1.73 mJ/m^2 by using W-FA-DM and W-FA-BN triples, respectively, which is in fact about 3.2 times higher than the γ_S^- obtained from the W-EG-DM triple. Obviously, 3.2 times difference in any physical property obtained from the exactly same sample could cause unacceptable scientific deviations, and thus our observations suggest that the SFE measurements should be performed on as much well-conditioned liquid triples as possible, and by providing mean data [14]. Therefore, we calculated the SFE components (γ_S^{LW}, γ_S^+, γ_S^-, γ_S^{AB}, and γ_S^{Tot}) of the TCO-based surfaces using the mean of the data obtained from W-FA-DM/BN, W-EG-DM/BN, W-GLY-DM/BN liquid triples (Table 2). Although van Oss-Chaudhury-Good method was effective for determining the SFE components of a surface, sometimes meaningless negative values can be seen in the square roots of γ_S^+ and γ_S^- [40,46,59]. In our work, such negative $\sqrt{\gamma_S^+}$ values were encountered during computations, and we assumed these values as zero in accordance with Robert J. Good's suggestion [59]. This trouble caused the γ_S^{AB} to be calculated as zero, and thus the contribution to the γ_S^{Tot} was only originated from the γ_S^{LW}component. Then, it becomes rather difficult to evaluate surface polarity since γ_S^{AB} represents the polar contribution of SFE [17]. Yet, van Oss-Chaudhury-Good method is still quite effective for understanding

Table 2
Values of the Lifshitz-van der Waals, acidic and basic components (mJ/m^2) of the TCO-based surfaces calculated by van Oss-Chaudhury-Good method.

Surface	γ_s^{LW}	γ_s^+	γ_s^-	γ_s^{AB}	γ_s^{Tot}
AZO	32.13	0.00	2.29	0.00	32.13
AZO/AZO	34.17	0.00	3.49	0.00	34.17
AZO/Ag	26.16	0.00	0.48	0.00	26.16
AZO/Ag/AZO	28.82	0.00	1.52	0.00	28.82
ITO	26.88	0.00	1.69	0.02	26.90
ITO/ITO	27.66	0.00	2.11	0.01	27.68
ITO/Ag	25.05	0.00	0.60	0.01	25.06
ITO/Ag/ITO	25.84	0.00	1.05	0.00	25.84
ZTO	25.56	0.00	1.36	0.02	25.58
ZTO/ZTO	26.34	0.01	1.46	0.08	26.43
ZTO/Ag	24.23	0.00	0.44	0.00	24.23
ZTO/Ag/ZTO	25.02	0.00	1.16	0.00	25.02

the acidity and basicity of the surfaces in terms of γ_S^+ and γ_S^- as given in Table 2. It is clearly seen that all the TCO surfaces show monopolar basic character because γ_S^+ values were found to be zero (or nearly zero) and quite small compared to the γ_S^- component [14].

The dispersive (γ_{SV}^d) and polar (γ_{SV}^p) components of the SFE were calculated by applying geometric (Owens and Wendt's method) [47] and harmonic (Wu's method) [48] mean approaches. The equation of the geometric mean (GM) approach can be written as,

$$\gamma_{LV}(1+\cos\theta) = 2\left(\sqrt{\gamma_{SV}^d\gamma_{LV}^d} + \sqrt{\gamma_{SV}^p\gamma_{LV}^p}\right) \quad (4)$$

The equation of the harmonic mean (HM) approach can be written as,

$$\gamma_{LV}(1+\cos\theta) = 4\left(\frac{\gamma_{SV}^d\gamma_{LV}^d}{\gamma_{SV}^d+\gamma_{LV}^d} + \frac{\gamma_{SV}^p\gamma_{LV}^p}{\gamma_{SV}^p+\gamma_{LV}^p}\right) \quad (5)$$

By solving the equation (4) for the GM approach and equation (5) for the HM approach, γ_{SV}^d and γ_{SV}^p components of the SFE were found. The DM and BN were chosen as the nonpolar liquids, and the W was selected as the polar liquid in evaluating the SFE components. The γ_{LV}^d and γ_{LV}^p values of the W, DM and BN liquids used in these equations were obtained from the literature [38,41,61] and given in Supplementary Material Table S6. Then, the total SFE (γ_S^{Tot}) of the surface was calculated as,

$$\gamma_S^{Tot} = \gamma_{SV}^d + \gamma_{SV}^p \quad (6)$$

The γ_{SV}^d, γ_{SV}^p, and γ_S^{Tot} results of the surfaces calculated from geometric and harmonic mean approaches using contact angle values of W-DM and W-BN liquid pairs are given in Supplementary Material Table S7, and the mean data obtained from these liquid pairs are listed in Table 3. As can be seen, the mean values obtained from GM approach and from van Oss-Chaudhury-Good method are similar. For example, the mean values for γ_S^{Tot}on AZO surface were calculated as 32.60 mJ/m^2 by using GM approach. Whereas, the mean values for γ_S^{Tot}on the same surface were calculated as 32.13 mJ/m^2 by using van Oss-Chaudhury-Good method. However, when using HM approach, the γ_S^{Tot}, γ_{SV}^d and γ_{SV}^p components of the SFE were found to be higher than the results obtained with GM approach (Table 3). For example, the mean values of the γ_S^{Tot} for AZO/Ag/AZO, ITO/Ag/ITO, and ZTO/Ag/ZTO were calculated as 32.45, 29.08, and 28.53 mJ/m^2, respectively by using HM approach. Whereas, the γ_S^{Tot} values for AZO/Ag/AZO, ITO/Ag/ITO, and ZTO/Ag/ZTO were calculated as 29.19, 26.05, and 25.28 mJ/m^2, respectively by using GM approach. As in Wu's previous determinations [48], these results show that the SFE components calculated by the HM approach are higher than the GM approach. On the other hand, no matter what the calculation approach is, all the SFE components of TCO/Ag/TCO surfaces were found to be lower than that of both TCO and TCO/TCO surfaces. These results point out that the presence of Ag interlayer resulted in a decrease of the SFE components. In order to explain this situation, the SFE components of the Ag interlayer were determined. The γ_S^{Tot}, γ_{SV}^p, and γ_{SV}^d for the Ag interlayer deposited on AZO surface were calculated as 26.20, 0.03, and 26.16 mJ/m^2, respectively by using the GM approach, indicating that the SFE components of the Ag interlayer were quite lower than the AZO, AZO/AZO, and AZO/Ag/AZO surfaces as given in Table 3.

Table 3
Surface free energy components (mJ/m^2) of the TCO-based surfaces calculated by geometric and harmonic mean approaches.

Surface	Geometric mean approach			Harmonic mean approach		
	γ_s^d	γ_s^p	γ_s^{Tot}	γ_s^d	γ_s^p	γ_s^{Tot}
AZO	32.13	0.47	32.60	33.21	2.64	35.84
AZO/AZO	34.17	0.85	35.01	35.01	3.75	38.76
AZO/Ag	26.16	0.03	26.20	28.04	0.32	28.36
AZO/Ag/AZO	28.82	0.38	29.19	30.31	2.13	32.45
ITO	26.88	0.42	27.30	28.66	2.12	30.78
ITO/ITO	27.66	0.36	28.03	29.33	1.98	31.32
ITO/Ag	25.05	0.11	25.17	27.10	0.81	27.91
ITO/Ag/ITO	25.84	0.21	26.05	27.77	1.31	29.08
ZTO	25.56	0.31	25.87	27.53	1.69	29.21
ZTO/ZTO	26.34	0.47	26.81	28.20	2.21	30.41
ZTO/Ag	24.23	0.05	24.28	26.40	0.34	26.74
ZTO/Ag/ZTO	25.02	0.26	25.28	27.07	1.45	28.53

In addition, it was found that the SFE values of AZO double coatings (AZO/AZO) were found to be higher than that of the AZO single layer surfaces as shown in Fig. 2. This is expected, because the growth of a TCO on the glass substrate, and the growth of the same TCO on an identical surface with itself are different processes, at least by means of the resultant morphology of the obtained surface. This result will be discussed later in more detail together with XRD and AFM analysis simultaneously in this work. Similar to AZO-based films, the γ_S^{Tot} values of ITO/Ag and ZTO/Ag surfaces were found to be lower than that of Ag interlayer free ITO- and ZTO-based surfaces as shown in Fig. 2. These results show that the presence of Ag interlayer that have lower SFE than TCO layers in thin films reduces the final SFE of the coating. In general, chemical composition, chemical heterogeneity, surface morphology, surface roughness, crystallographic orientation, molecular polarizability and electrostatic interactions are the main factors affecting the SFE value of a solid surface when measurements are conducted under the same conditions [14,38,49]. Thus, a detailed crystallographic and morphological analysis is necessary to make clarify the effect of Ag interlayer presence on the SFE properties of TCOs.

SFE depends on the number of broken bonds on the surface. Obviously, the surface atoms are not bonded to their maximum number of nearest neighbors, and their coordination numbers are not same with the coordination numbers of bulk atoms. This means that structural ordering and percentage crystallinity should dictate the SFE. Besides, even in the same crystal structure, the crystallographic orientation also effects the SFE, since the coordination numbers of surface atoms on different crystallographic planes are not always equal. Fig. 3 shows the grazing incidence XRD measurement results of double layer oxides and TCO/Ag/TCO films. As can be seen in this figure, AZO shows a polycrystalline nature with hexagonal wurtzite structure, having diffraction peaks associated with the zinc oxide (0 0 2), (1 0 2) and (1 0 3) planes, where the (0 0 2) peak being the most intense in both the spectra of AZO/AZO and AZO/Ag/AZO (JCPDS File No. 00–036-1451). The peaks (1 0 0), (1 0 1) and (1 1 0) are also realized with a very low intensity in the spectra of AZO/AZO while it is not distinguishable when Ag was deposited between two AZO layers as seen in Fig. 3(a). Besides, an intense crystalline peak at about 38° was observed in all TCO/Ag/TCO films, and the peak was ascribed to the (1 1 1) peak of Ag, expressing the successful deposition of Ag as the interlayer. Similar to AZO-based films, ITO/ITO and ITO/Ag/ITO films were also seen to be polycrystalline with cubic bixbyite In_2O_3. The diffraction peaks at about 30°, 35° and 50° are ascribed to (2 2 2), (4 0 0) and (4 4 0) peaks of ITO, respectively (JCPDS File No. 71–2195). The intensities of ITO peaks are found to be

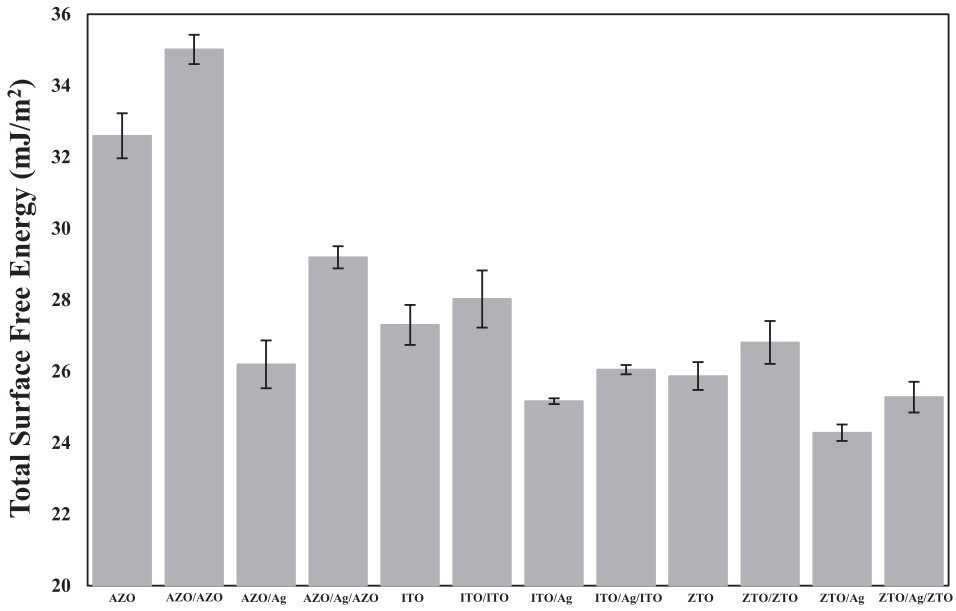

Fig. 2. Comparison of total surface free energy values of TCO, TCO/TCO, TCO/Ag, and TCO/Ag/TCO surfaces calculated by geometric mean approach.

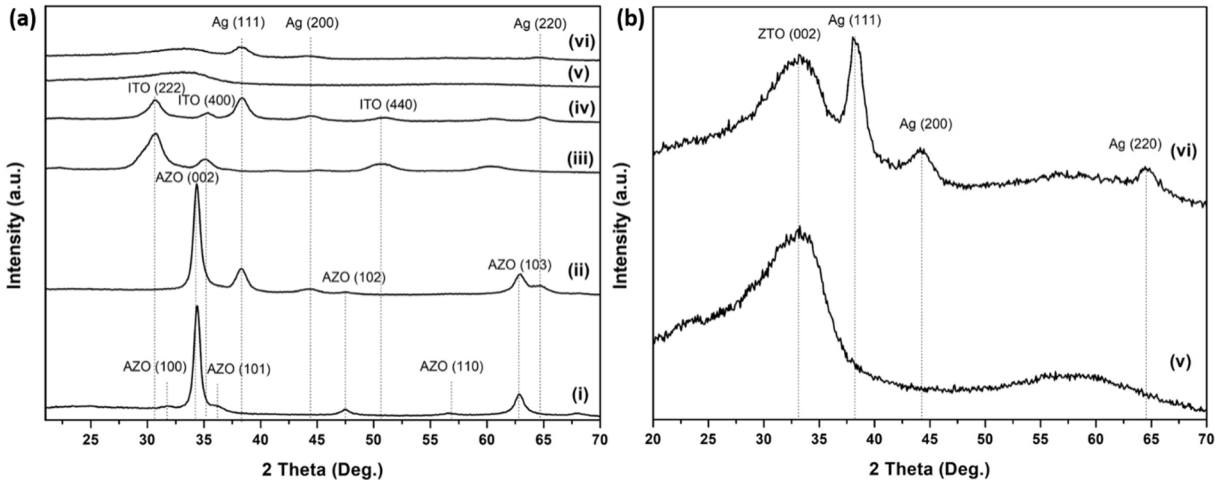

Fig. 3. Grazing incidence XRD patterns of (a) TCO/TCO and TCO/Ag/TCO films (i) AZO/AZO, (ii) AZO/Ag/AZO, (iii) ITO/ITO, (iv) ITO/Ag/ITO, (v) ZTO/ZTO, (vi) ZTO/Ag/ZTO, (b) ZTO/ZTO (v) and ZTO/Ag/ZTO (vi) films.

decreasing with the Ag interlayer deposition. This situation is related to the decreasing ratio of ITO in the overall film. Although we report a preferred orientation along (400) in the top ITO film when Au was inserted as the interlayer in our previous works [14,62], no such effect was observed for the Ag interlayer in any of the TCOs that studied in the present work. This might be attributed to the SFE and surface polarity differences between the Au and Ag interlayers. Both the total SFE value and surface polarity of Au interlayer is higher than Ag interlayer [14]. XRD patterns of ZTO/ZTO and ZTO/Ag/ZTO are plotted in Fig. 3(b), which suggest only partial crystallinity of ZTO due to a very broad amorphous peak through (002) plane at about 33°.

Combining the XRD patterns with the SFE results, one could expect that the SFE results should be correlated with the atomic structure in the multilayered films. For instance, the SFE results of double TCO coatings were found to be higher than that of single layer coatings as aforementioned previously (Fig. 2). Moreover, this SFE differences between the single layer and double layered TCOs were found to be lowest in the ZTO films (Fig. 2). In fact, this observation is persistent with the XRD results in Fig. 3, which also suggest that the percentage crystallinity of the ZTO is much lower than both AZO and ITO. Comparing the deposition of a TCO on a glass substrate with its deposition on another identical TCO layer, one could notice that the atomic distribution on the surface of amorphous glass substrate and the crystalline TCO layer must be different. Accordingly, the deposition of the secondary TCO layer on the initial TCO film would result in better bonding and higher SFE as comparing to the deposition of that TCO on the amorphous glass.

Apart from structural analysis, surface topography is also important in the accurate evaluation of surface properties. Surface morphology effects the SFE results since the number of broken bonds on a particular surface depends for instance on roughness, homogeneity of the surface, as well as the distinctive position and amount of surface intrusions and protrusions. Therefore, a topographical study was conducted by AFM, as can be seen in Fig. 4, to better comment on the wettability differences between the as-prepared samples. The RMS roughness values that determined through AFM analysis illustrate that all of the single layered TCOs are actually smooth with roughness values changing between 1.47 and 1.80 nm (Table S1). Also, all of the double-layered coatings provided lower RMS roughness values comparing to single layered ones. Similar to the SFE differences between single and double layered TCOs, the deposition of a TCO on an identical, crystalline TCO layer and the

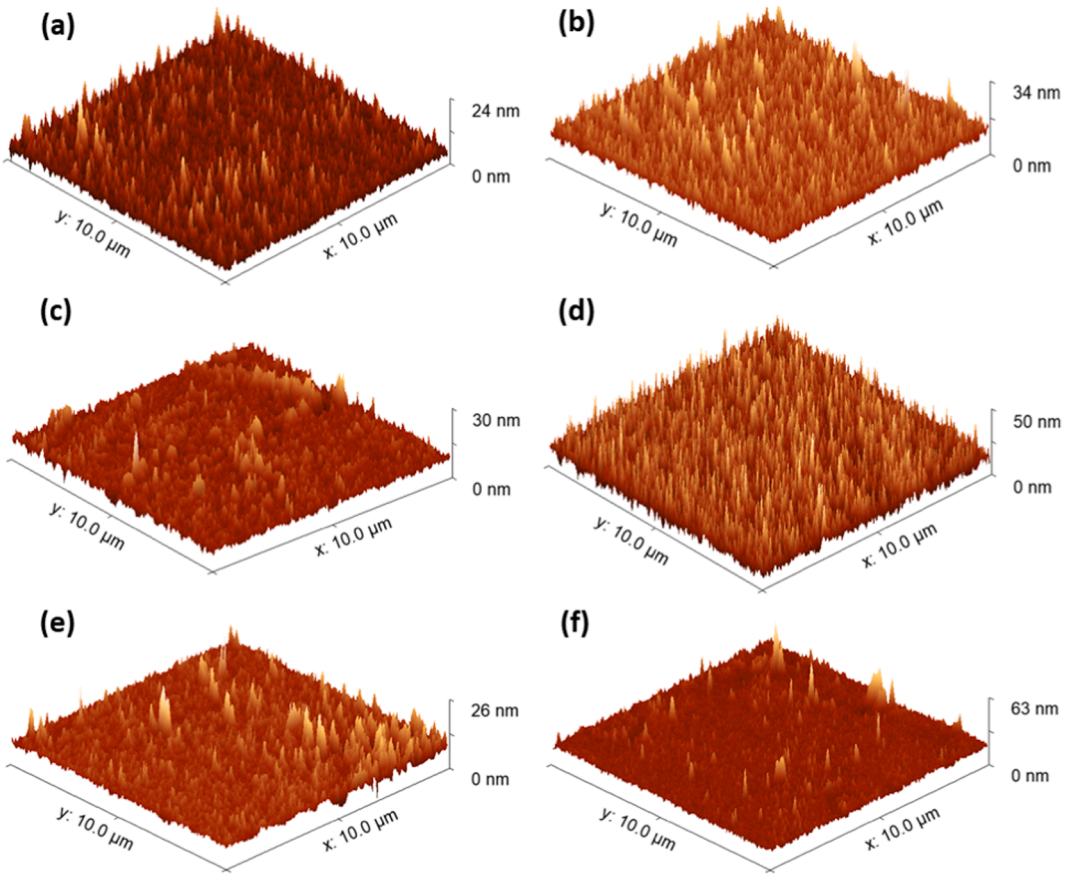

Fig. 4. 3D AFM images of (a) AZO, (b) AZO/Ag/AZO, (c) ITO, (d) ITO/Ag/ITO (e) ZTO, (f) ZTO/Ag/ZTO.

deposition of that TCO on an amorphous glass substrate are different phenomenon. It could be expected that the deposition of a TCO on an identical substrate would provide better cohesion and matching comparing to the use of a glass substrate, and thus, growth of the top TCO would be more homogeneous, providing a smoother surface. Interestingly, the AFM results illustrate that the surface roughness of TCO/Ag films strongly depend on the TCOs (Fig. S2 and Table S1). While Ag films on ITO and AZO films were much smoother, its deposition on ZTO cause formation of a rough surface (Fig. S2). This might be due to the lower crystallinity of ZTOs, causing Ag atoms to agglomerate on the ZTO surface, and thus deteriorating the surface properties. In fact, one of the main factors behind the texture and morphology of a film was reported to be substrate-adatom interactions [63,64]. In this context, many reports mentioned the effect of substrate crystallinity on the film morphology [65–67]. For instance, Yoon et al. prepared $BaTiO_3$ films on Si, InSb and ITO-coated glass substrates and reported that the topography of the deposited films strongly depend on the substrate crystallinity, especially for high temperature depositions [67]. Although the deposition temperatures are low in this work, they are in fact kept same for all different TCO-based structures studied here. Also, calculated SFE results indicate that the SFE differences between the ZTO and ITO is not that dramatic. All of these suggest that the reason behind the poor surface morphology of Ag interlayer in the case of ZTO seems to be the limited ordering of the surface atoms in the ZTO-bottom layer, which might affect the morphology of the Ag interlayer as the interactions between the disordered surface atoms of ZTO and ordered surface atoms of Ag might favor definitive orientations in the Ag structure, might cause Ag agglomerations and the formation of a rougher surface. Overall, as can be seen in Fig. 4 that the introduction of Ag interlayer increases the roughness values on the surface of sandwich films considerably.

3.2. Estimation of the work of adhesion between TCOs and Ag interlayer

One way to decrease electrical resistivity of TCOs involves preparation of sandwich structures by inserting a metal film between the TCO layers. The thickness of the metal interlayer kept relatively small in these systems in order not to sacrifice much of the transparency. Metals such as Au, Ag, Cu and Al are widely used as the interlayer film in such TCO/metal/TCO sandwich structures [2,3,68]. Among them, Ag offers the highest conductivity as well as the lowest absorption coefficient and refractive index in the visible region, and thus becomes the ideal candidate in terms of the trade-off between transparency and conductivity [13,69]. Yet, it is important to note that TCO/metal/TCO structures should also possess high thermal stability. This is simply because they are usually subjected to post-deposition heat treatments to further improve optical and electrical properties. The annealing process provides crystallite growth, and thus carrier mobility is enhanced as a result of less scattering, in addition to an improvement in carrier concentration thanks to better extrinsic doping and formation of oxygen vacancies [2,70,71]. However, oxidation of Ag is reported during the annealing, as well as the agglomeration of Ag, which disrupts film continuity due to the growth of Ag islands [2,72–75]. Oxygen diffusion both at the Ag/TCO interface and from the annealing atmosphere decreases the purity of Ag, and thus both electrical conductivity and optical transparency drops through increase of carrier and photon scattering [75–78]. Accordingly, the annealing should be conducted in vacuum or nitrogen in the case of TCO/Ag/TCO structures, adding extra difficulty and cost. What's more, previous reports indicate that the electrical and optical properties of TCO/Ag/TCOs start to decay when annealing temperature increased above 450 °C even when the annealing is conducted in vacuum or nitrogen [2,76,77]. Likewise, the humidity stability of Ag is also problematic and TCO/Ag/TCO structures are not stable under moisture

attack [2]. Aggregation and/or migration of Ag atoms under humidity causes the agglomeration of Ag interlayer and disrupts the TCO layer, resulting in the loss of electrical and optical performance in like manner with the afore-mentioned explanations for thermal stability [2,79–81]. Obviously, Au becomes the best option in this regard due to its excellent thermal and humidity stability. In fact, Au is the least reactive metal and its oxides are not stable. The Au is even mined in its pure form from Earth's crust while other metals necessitate various processes for extraction from their ores. Accordingly, previous reports on TCO/Au/TCO structures also indicate that such structures are stable and maintain their electrical and optical performance as expected, for instance when subjected to a moist atmosphere with a relative humidity of 90% at 60 °C for 600 h [82]. Another important point in TCO/metal/TCO structures should be their mechanical stability and flexibility since they are also considered in flexible electronic devices such as in organic luminescent displays (OLED), liquid crystal displays (LCD), capacitors, etc. The incorporation of a metal interlayer improves the mechanical stability in this regard comparing to a single TCO layer due mainly to the ductility of the metal interlayer, which helps the TCO/metal/TCO structure to maintain a high electrical conductivity even beyond the failure strain of the TCOs [83,84]. Apparently, adhesion strength of the metal interlayer plays a key role for mechanical stability, especially in flexible electronics.

We calculated work of adhesion (W_a) between TCOs and the Ag interlayer to comment on the adhesion strength of the as-prepared sandwich structures. The W_a values for both top and bottom TCO films to the Ag interlayer were determined by applying Girifalco-Good equations [53] to the SFE values obtained by geometric and harmonic mean approaches. The main equation of Girifalco-Good can be written for our surfaces as:

$$W_a = 2\phi\sqrt{\gamma_{TCO}\gamma_{Ag}} \tag{7}$$

where γ_{TCO} is SFE of the TCO, γ_{Ag} is SFE of the Ag interlayer, and ϕ is the interaction parameter of interphase. According to the procedure given by Souheng Wu [54], by combining the geometric mean equation [47] and Girifalco-Good equation [53], the ϕ value of the interphase between TCO and Ag can be written as,

$$\phi = \sqrt{X^d_{TCO}X^d_{Ag}} + \sqrt{X^p_{TCO}X^p_{Ag}} \tag{8}$$

where X^d_j denotes dispersive component fraction of the SFE, X^p_j denotes polar component fraction of the SFE, subscript j represents the material (TCO or Ag), and $X^d_j + X^p_j = 1$.

By combining the harmonic mean [48] and Girifalco-Good equations [53], the ϕ value of the interphase between TCO and Ag can be written as [54],

$$\phi = 2\left(\frac{X^d_{TCO}X^d_{Ag}}{g_{TCO}X^d_{TCO} + g_{Ag}X^d_{Ag}} + \frac{X^p_{TCO}X^p_{Ag}}{g_{TCO}X^p_{TCO} + g_{Ag}X^p_{Ag}}\right) \tag{9}$$

The parameters in the equation (8) and (9) were calculated as,

$$X^d_j = \frac{\gamma^d_j}{\gamma_j} \tag{10}$$

$$X^p_j = \frac{\gamma^p_j}{\gamma_j} \tag{11}$$

$$g_{j1} = \sqrt{\gamma_{j1}/\gamma_{j2}} \tag{12}$$

By solving the equation (8) for the GM approach, and the equation (9) for the HM approach, the ϕ values were found. Then, the W_a values for TCO films to the Ag interlayer were calculated using equation (7).

The W_a values between TCO layers and Ag interlayer are given in Table 4. The W_a of a TCO film to Ag interlayer varied from 49.5 to 61.9 mJ/m^2 depending on the type of TCO and calculation model. The W_a in ITO/Au/ITO is also calculated using the data given in our previous work [14] and its results are also listed in Table 4, since Au is the other promising interlayer material as explained above. The W_a of the ITO film to Au interlayer varied from 72.6 to 84.8 mJ/m^2. Whereas, the W_a values between ITO and Ag interlayer varied from 51.2 to 58.1 mJ/m^2. The results show that the adhesion between Au and ITO is much better comparing to the adhesion of Ag. Atomic structure, electronic structure, bonding strength and surface quality are particularly important in adhesion of TCOs and interlayers. In fact, both Au and Ag are FCC crystals with very similar lattice constants (JCPDS 4-0783 and 4-0784), and both having most intense XRD peaks of (1 1 1) planes at about 2θ = 38.1°. The surface roughness of the interlayers is again almost similar in this work and in our previous works [14,62]. As per electronic configuration, both Ag and Au are group 1B elements with only 1 valence electron and have similar configurations. Yet, electronegativity of Au (2.54) is higher than Ag (1.93), which could contribute to a higher bonding strength, and thus better adhesion. Besides, Au is the noblest of all metals, and is extremely stable as explained above. This might also contribute to the very high work of adhesion at the Au/ITO interface comparing to the Ag/ITO. Oxygen might diffuse to some extent through the Ag at the Ag/TCO interface in the case of Ag interlayer, causing the agglomeration of Ag layer and reducing its adhesion. Regarding the work of adhesion comparison of various Ag/TCOs, Table 4 shows that AZO provides the best adhesion to reach a better mechanical stability.

Table 4
Work of adhesion (mJ/m^2) values of the TCOs to silver and gold interlayer calculated by geometric and harmonic mean approaches.

Interface	W_a (GM method)	W_a (HM method)
Top AZO-silver	55.1	59.4
Bottom AZO-silver	58.2	61.9
Top ITO-silver	51.2	56.9
Bottom ITO-silver	52.3	58.1
Top ZTO-silver	49.5	54.6
Bottom ZTO-silver	50.0	55.0
Top ITO-gold[a]	74.6	84.8
Bottom ITO-gold[a]	72.6	82.3

[a] : Calculated from the data given in reference [14].

To comment more on the adhesion behavior, film qualities are further evaluated through SEM analysis in Fig. 5. Strikingly, SEM results signify that the Ag interlayer quality is extremely poor in the case of ZTO, which is in good accordance with the W_a calculations. In fact, we report that a continuous Ag film with approximately 10 nm thickness could be realized both on AZO (ca 39 nm) and ITO (ca 42 nm) bottom layers. Besides, the top AZO and ITO layers on the Ag interlayer are also found to be symmetrical with the bottom layers. However, the Ag film continuity seems to be problematic with agglomerations in the case of ZTO. The thickness of the aggregates was measured as 10–20 nm. Although the deposition time was same for the deposition of Ag films in all TCOs, increasing Ag thickness in ZTO show that Ag particles arriving to the ZTO film preferentially deposited on another Ag particle instead of ZTO. This might also be effected by the lower percentage crystallinity of ZTO comparing to AZO and ITO as can be inferred from the XRD patterns in Fig. 3, considering that Ag has FCC structure. Moreover, unlike AZO and ITO, the thicknesses of bottom and top ZTO layers are not symmetrical with about 25–30, and 50 nm thicknesses for the top and bottom films, respectively (Fig. 5). On the other hand, due to the non-continuous Ag interlayer, the top ZTO film is not continuous as well. Besides, the top ZTO even seem to be in contact with the bottom ZTO at some regions as highlighted in Fig. S3. Considering this, the thickness of the top layer might be thought as the total film thickness just above the bottom ZTO, or in other words the top layer might be in between 35 and 50 nm. As can be seen in Fig. S3, if the thickness of top ZTO is measured from the ZTO-ZTO contact points, top and bottom ZTO layers might even look symmetrical. Overall, these observations are in good accordance with both SFE and W_a calculations. However, we must note that

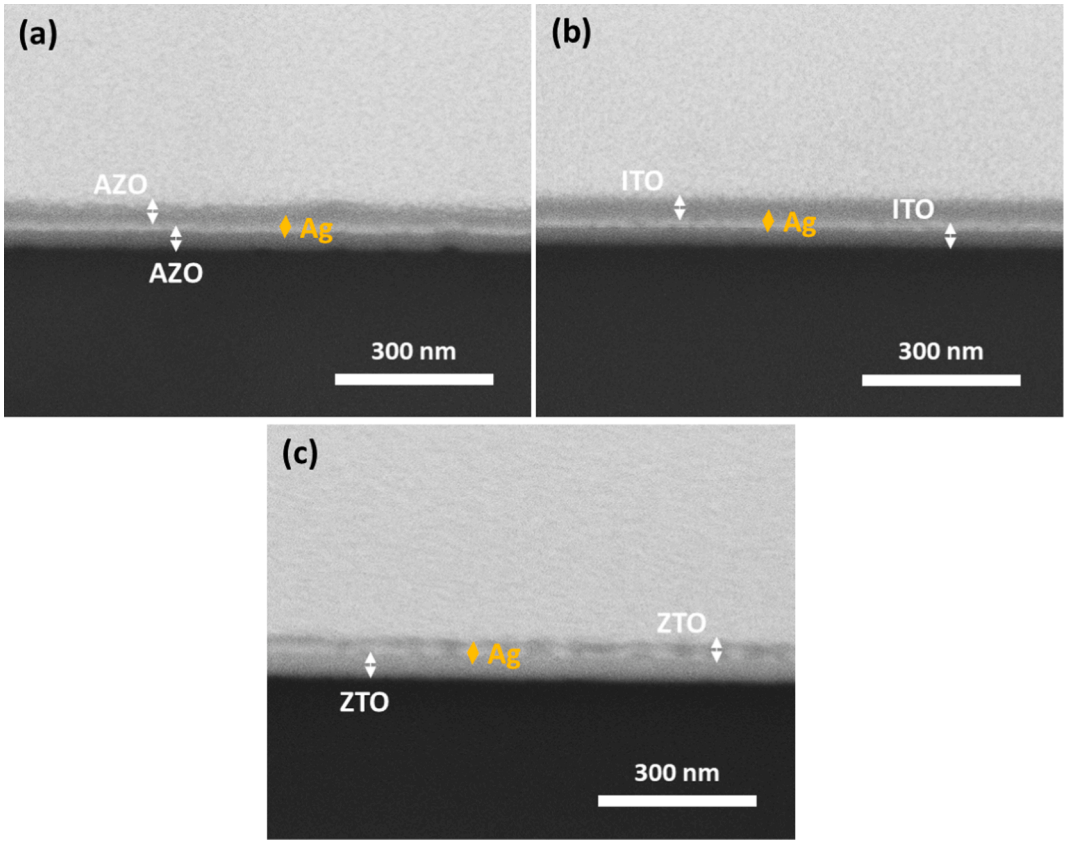

Fig. 5. Cross section SEM images of (a) AZO/Ag/AZO, (b) ITO/Ag/ITO, (c) ZTO/Ag/ZTO.

the above-given explanations in interlayer selection regarding electrical and optical properties as well as the thermal and humidity stability should also be considered in the selection of optimum TCOs for the specific applications at hand. In this regard, ITO not only provides the best combination of transparency and conductivity, but also has better thermal and humidity stability comparing to AZO [85–88]. For instance, 40 nm ITO/15 nm Ag/40 nm ITO on glass substrate provides a sheet resistance of 4.2 ohm/sq and optical transmittance of 85% [85], while 40 nm AZO/16 nm Ag/40 nm AZO on glass substrate provides a sheet resistance of ~5 ohm/sq and optical transmittance of ~82% [86]. Regarding thermal and humidity stability, while ITO is stable in Ar atmosphere until 900 °C, and stable in air until temperature reaches about 800 °C, AZO is stable in Ar atmosphere until 600 °C, and in air until temperature reaches about 350–400 °C [87,88]. Another interesting observation in Table 4 is that the W_a between metal interlayer and bottom and top TCOs are slightly different. Naturally, this could be originated from the SFE differences between top and bottom TCOs. Although bottom TCOs are deposited on the substrates, the top TCOs are grown on the metallic interlayers. Accordingly, the surface morphology of the top TCOs are not same with the bottom TCOs as can be also understood from the AFM images shown in Fig. 4. All in all, the SFE between interlayers should be controlled by various surface treatments in such a way that the W_a values are balanced to prepare more stable and durable sandwich structures in the future.

4. Conclusions

A detailed SFE knowledge is vital in evaluating the adhesion, adsorption, wettability and lubrication behavior of any given surface, and thus to design structures with specific surface properties for adapting various needs. This is particularly important for sandwich structures as such systems have many interfaces, and the adhesion between these layers should be appropriate to satisfy an acceptable service performance. In this context, we conducted a detailed SFE analysis of the TCO-based structures with Ag interlayer by acid-base, geometric mean and harmonic mean approaches. To do this, apparent contact angle measurements of seven different liquids having various surface tension values were performed by the sessile drop method. As well as the SFE, work of adhesion between the TCOs and Ag interlayers were also determined based on the Dupré, Fowkes and Girifalco-Good equations. The theoretical SFE and work of adhesion results were discussed in combination with material characterization tools to provide a comprehensive analysis. We report that the calculation methods and selected liquid pairs affect the SFE values for the same surface significantly. According to the calculations, the SFE values of the TCOs decrease in the following order: AZO > ITO > ZTO, and the SFE components of the TCO/Ag/TCO sandwich films are lower than that of TCO surfaces due to the presence of Ag interlayer. Also, we report that the structural ordering and percentage crystallinity, as well as the morphology of the deposited films strongly influence the SFE results since they both effect the number of broken bonds for the surface atoms. Significantly, W_a results indicate that the adhesion between AZO and Ag were found to be stronger than that of both ITO/Ag and ZTO/Ag interfaces. In addition, we observed that the adhesion between Au interlayer and ITO is stronger than ITO/Ag interface due to the higher electronegativity and stability of Au. Overall, this study demonstrates that desirable sandwich structures with excellent adhesion properties could be reached simply by controlling the SFE properties of the interlayers.

CRediT authorship contribution statement

Salih Ozbay: Conceptualization, Formal analysis, Methodology, Investigation, Visualization, Writing – original draft, Writing – review & editing, Supervision. **Nursev Erdogan:** Formal analysis, Investigation, Visualization, Writing – review & editing. **Fuat Erden:** Formal analysis, Writing – original draft, Writing – review & editing. **Merve**

Ekmekcioglu: Investigation. **Busra Rakop:** Formal analysis. **Mehtap Ozdemir:** Writing – review & editing. **Gulnur Aygun:** Writing – review & editing. **Lutfi Ozyuzer:** Resources, Writing – review & editing.

Declaration of Competing Interest

The authors declare that they have no known competing financial interests or personal relationships that could have appeared to influence the work reported in this paper.

Acknowledgement

This work was partially supported by Scientific and Technological Research Council of Turkey (No: 5189901 and 20AG001) and Research Foundation of Turkish Aerospace (No: TM0131).

Appendix A. Supplementary data

Supplementary data to this article can be found online at https://doi.org/10.1016/j.apsusc.2021.150901.

References

[1] K.L. Chopra, S. Major, D.K. Pandya, Transparent conductors-A status review, Thin Solid Films 102 (1983) 1–46.
[2] C. Guillén, J. Herrero, TCO/metal/TCO structures for energy and flexible electronics, Thin Solid Films 520 (2011) 1–17.
[3] K.H. Choi, J.Y. Kim, Y.S. Lee, H.J. Kim, ITO/Ag/ITO multilayer films for the application of a very low resistance transparent electrode, Thin Solid Films 341 (1999) 152–155.
[4] H. Ferhati, F. Djeffal, A. Benhaya, Optimized high-performance ITO/Ag/ITO multilayer transparent electrode deposited by RF magnetron sputtering, Superlattices Microstruct. 129 (2019) 176–184.
[5] C. Guillén, J. Herrero, Transparent conductive ITO/Ag/ITO multilayer electrodes deposited by sputtering at room temperature, Opt. Commun. 282 (2009) 574–578.
[6] D. Miao, S. Jiang, S. Shang, Z. Chen, Infrared reflective properties of AZO/Ag/AZO trilayers prepared by RF magnetron sputtering, Ceram. Int. 40 (2014) 12847–12853.
[7] M. Ekmekcioglu, N. Erdogan, A.T. Astarlioglu, S. Yigen, G. Aygun, L. Ozyuzer, M. Ozdemir, High transparent, low surface resistance ZTO/Ag/ZTO multilayer thin film electrodes on glass and polymer substrates, Vacuum 187 (2021), 110100.
[8] F. Li, Y. Zhang, C. Wu, Z. Lin, B. Zhang, T. Guo, Improving efficiency of organic light-emitting diodes fabricated utilizing AZO/Ag/AZO multilayer electrode, Vacuum 86 (2012) 1895–1897.
[9] S.Y. Lee, Y.S. Park, T.Y. Seong, Optimized ITO/Ag/ITO multilayers as a current spreading layer to enhance the light output of ultraviolet light-emitting diodes, J. Alloys Compd. 776 (2019) 960–964.
[10] H. Wang, C. Tang, Q. Shi, M. Wei, Y. Su, S. Lin, M. Dai, Influence of Ag incorporation on the structural, optical and electrical properties of ITO/Ag/ITO multilayers for inorganic all-solid-state electrochromic devices, Ceram. Int. 47 (2021) 7666–7673.
[11] T. Winkler, H. Schmidt, H. Flügge, F. Nikolayzik, I. Baumann, S. Schmale, T. Weimann, P. Hinze, H.H. Johannes, T. Rabe, S. Hamwi, T. Riedl, W. Kowalsky, Efficient large area semitransparent organic solar cells based on highly transparent and conductive ZTO/Ag/ZTO multilayer top electrodes, Org. Electron. 12 (2011) 1612–1618.
[12] K.P. Sibin, N. Selvakumar, A. Kumar, A. Dey, N. Sridhara, H.D. Shashikala, A. K. Sharma, H.C. Barshilia, Design and development of ITO/Ag/ITO spectral beam splitter coating for photovoltaic-thermoelectric hybrid systems, Sol. Energy. 141 (2017) 118–126.
[13] K.P. Sibin, G. Srinivas, H.D. Shashikala, A. Dey, N. Sridhara, A.K. Sharma, H. C. Barshilia, Highly transparent and conducting ITO/Ag/ITO multilayer thin films on FEP substrates for flexible electronics applications, Sol. Energy Mater. Sol. Cells. 172 (2017) 277–284.
[14] S. Ozbay, N. Erdogan, F. Erden, M. Ekmekcioglu, M. Ozdemir, G. Aygun, L. Ozyuzer, Surface free energy analysis of ITO/Au/ITO multilayer thin films on polycarbonate substrate by apparent contact angle measurements, Appl. Surf. Sci. 529 (2020), 147111.
[15] S.K. So, W.K. Choi, C.H. Cheng, L.M. Leung, C.F. Kwong, Surface preparation and characterization of indium tin oxide substrates for organic electroluminescent devices, Appl. Phys. A Mater. Sci. Process. 68 (1999) 447–450.
[16] J.S. Kim, R.H. Friend, F. Cacialli, Surface energy and polarity of treated indium-tin-oxide anodes for polymer light-emitting diodes studied by contact-angle measurements, J. Appl. Phys. 86 (1999) 2774–2778.
[17] Z. Zhong, S. Yin, C. Liu, Y. Zhong, W. Zhang, D. Shi, C. Wang, Surface energy for electroluminescent polymers and indium-tin-oxide, Appl. Surf. Sci. 207 (2003) 183–189.
[18] Z.Z. You, J.Y. Dong, Surface modifications of ITO electrodes for polymer light-emitting devices, Appl. Surf. Sci. 253 (2006) 2102–2107.
[19] T. Kawai, Y. Maekawa, M. Kusabiraki, Plasma treatment of ITO surfaces to improve luminescence characteristics of organic light-emitting devices with dopants, Surf. Sci. 601 (2007) 5276–5279.
[20] M. Shekargoftar, R. Krumpolec, T. Homola, Enhancement of electrical properties of flexible ITO/PET by atmospheric pressure roll-to-roll plasma, Mater. Sci. Semicond. Process. 75 (2018) 95–102.
[21] H.S. Im, S.K. Kim, T.J. Lee, T.Y. Seong, Combined effects of oxygen pressures and RF powers on the electrical characteristics of ITO-based multilayer transparent electrodes, Vacuum 169 (2019), 108871.
[22] N.R. Armstrong, C. Carter, C. Donley, A. Simmonds, P. Lee, M. Brumbach, B. Kippelen, B. Domercq, S. Yoo, Interface modification of ITO thin films: Organic photovoltaic cells, Thin Solid Films 445 (2003) 342–352.
[23] S. Vunnam, K. Ankireddy, J. Kellar, W. Cross, Surface modification of indium tin oxide for direct writing of silver nanoparticulate ink micropatterns, Thin Solid Films 531 (2013) 294–301.
[24] M.H. Jung, H.S. Choi, Surface treatment and characterization of ITO thin films using atmospheric pressure plasma for organic light emitting diodes, J. Colloid Interface Sci. 310 (2007) 550–558.
[25] G. Lee, E. Park, V.T. Nguyen, S. Heo, N.A. Nguyen, L.L. Larina, I. Yoon, H.S. Choi, Plasma-assisted ITO sol coating for optimizing the optoelectronic properties of ITO glass, Appl. Surf. Sci. 551 (2021), 149414.
[26] S.G. Jung, K.B. Choi, C.H. Park, Y.S. Shim, C.H. Park, Y.W. Park, B.K. Ju, Effects of Cl2 plasma treatment on stability, wettability, and electrical properties of ITO for OLEDs, Opt. Mater. 93 (2019) 51–57.
[27] Y.T. Cheng, J.J. Ho, C.K. Wang, W. Lee, C.C. Lu, B.S. Yau, J.L. Nain, S.H. Chang, C. C. Chang, K.L. Wang, Improvement of organic solar cells by flexible substrate and ITO surface treatments, Appl. Surf. Sci. 256 (2010) 7606–7611.
[28] W.J. Dong, J.Y. Park, J. Ham, G.H. Jung, I. Lee, J.L. Lee, Dual Effect of ITO-Interlayer on Inverted Top-Illuminated Polymer Solar Cells: Wetting of Polyelectrolyte and Tuning of Cavity, Adv. Funct. Mater. 26 (2016) 5437–5446.
[29] J. Davenas, S. Besbes, A. Abderrahmen, N. Jaffrezic, H. Ben Ouada, Surface characterisation and functionalisation of indium tin oxide anodes for improvement of charge injection in organic light emitting diodes, Thin Solid Films 516 (2008) 1341–1344.
[30] S. Besbes, H. Ben Ouada, J. Davenas, L. Ponsonnet, N. Jaffrezic, P. Alcouffe, Effect of surface treatment and functionalization on the ITO properties for OLEDs, Mater. Sci. Eng. C. 26 (2006) 505–510.
[31] A. Arazna, G. Koziol, K. Janeczek, K. Futera, W. Stęplewski, Investigation of surface properties of treated ITO substrates for organic light-emitting devices, J. Mater. Sci. Mater. Electron. 24 (2013) 267–271.
[32] N. Gupta, S. Sasikala, D.B. Mahadik, A.V. Rao, H.C. Barshilia, Dual-scale rough multifunctional superhydrophobic ITO coatings prepared by air annealing of sputtered indium-tin alloy thin films, Appl. Surf. Sci. 258 (2012) 9723–9731.
[33] H.K. Park, S.W. Yoon, W.W. Chung, B.K. Min, Y.R. Do, Fabrication and characterization of large-scale multifunctional transparent ITO nanorod films, J. Mater. Chem. A. 1 (2013) 5860–5867.
[34] J. Kim, D. Lee, S. Song, S.Y. Cho, J.S. Bae, W. Kim, B.H. Youn, Y. Kim, J.S. Lee, S. D. Bu, S. Park, Surface chemistry modification in ITO films induced by Sn^{2+} ionic state variation, Curr. Appl. Phys. 17 (2017) 1415–1421.
[35] K.H. Patel, S.K. Rawal, Influence of power and temperature on properties of sputtered AZO films, Thin Solid Films 620 (2016) 182–187.
[36] S. Jiang, J. Xu, D. Miao, L. Peng, S. Shang, P. Zhu, Water-repellency, ultraviolet protection and infrared emissivity properties of AZO film on polyester fabric, Ceram. Int. 43 (2017) 2424–2430.
[37] I. Saafi, T. Larbi, A. Amlouk, M. Amlouk, Physical investigations and DFT model calculation on Zn_2SnO_4-ZnO (ZTO-ZO) alloy thin films for wettability and photocatalysis purposes, Optik. 187 (2019) 49–64.
[38] H.Y. Erbil, Surface Chemistry of Solid and Liquid Interfaces, Blackwell Publishing, Oxford, 2006.
[39] C.C. Ho, M.C. Khew, Surface free energy analysis of natural and modified natural rubber latex films by contact angle method, Langmuir 16 (2000) 1407–1414.
[40] J.W. Drelich, L. Boinovich, E. Chibowski, C. Della Volpe, L. Hołysz, A. Marmur, S. Siboni, Contact angles: History of over 200 years of open questions, Surf. Innov. 8 (2020) 3–27.
[41] D.Y. Kwok, The usefulness of the Lifshitz-van der Waals/acid-base approach for surface tension components and interfacial tensions, Colloids Surfaces A Physicochem. Eng. Asp. 156 (1999) 191–200.
[42] D.Y. Kwok, A.W. Neumann, Contact angle measurement and contact angle interpretation, Adv. Colloid Interface Sci. 81 (1999) 167–249.
[43] D.Y. Kwok, A.W. Neumann, Contact angle interpretation in terms of solid surface tension, Colloids Surfaces A Physicochem. Eng. Asp. 161 (2000) 31–48.
[44] C. Della Volpe, D. Maniglio, S. Siboni, M. Morra, Recent theoretical and experimental advancements in the application of van Oss-Chaudury-Good acid-base theory to the analysis of polymer surfaces I. General aspects, J. Adhes. Sci. Technol. 17 (2003) 1477–1505.
[45] C. Della Volpe, D. Maniglio, M. Brugnara, S. Siboni, M. Morra, The solid surface free energy calculation: I. In defense of the multicomponent approach, J. Colloid Interface Sci. 271 (2004) 434–453.
[46] H.Y. Erbil, The debate on the dependence of apparent contact angles on drop contact area or three-phase contact line: A review, Surf. Sci. Rep. 69 (2014) 325–365.
[47] D.K. Owens, R.C. Wendt, Estimation of the surface free energy of polymers, J. Appl. Polym. Sci. 13 (1969) 1741–1747.
[48] S. Wu, Calculation of interfacial tension in polymer systems, J. Polym. Sci. Part C Polym. Symp. 34 (1971) 19–30.

[49] C.J. van Oss, M.K. Chaudhury, R.J. Good, Interfacial Lifshitz-van der Waals and polar interactions in macroscopic systems, Chem. Rev. 88 (1988) 927–941.
[50] A. Dupré, P. Dupré, Théorie méchanique de la chaleur, Gauthier-Villars, Paris, 1869.
[51] F.M. Fowkes, Determination of interfacial tensions, contact angles, and dispersion forces in surfaces by assuming additivity of intermolecular interactions in surfaces, J. Phys. Chem. 66 (1962) 382.
[52] F.M. Fowkes, Attractive forces at interfaces, Ind. Eng. Chem. 56 (1964) 40–52.
[53] L.A. Girifalco, R.J. Good, A theory for the estimation of surface and interfacial energies. I. Derivation and application to interfacial tension, J. Phys. Chem. 61 (1957) 904–909.
[54] S. Wu, Polymer Interface and Adhesion, Marcel Dekker, New York, 1982.
[55] A.N. Kolodin, A.I. Bulavchenko, Contact angle and free surface energy of CdS films on polystyrene substrate, Appl. Surf. Sci. 463 (2019) 820–828.
[56] S. Ozbay, H.Y. Erbil, Superhydrophobic and oleophobic surfaces obtained by graft copolymerization of perfluoroalkyl ethyl acrylate onto SBR rubber, Colloids Surfaces A Physicochem. Eng. Asp. 481 (2015) 537–546.
[57] C.J. van Oss, R.J. Good, M.K. Chaudhury, Additive and nonadditive surface tension components and the interpretation of contact angles, Langmuir 4 (1988) 884–891.
[58] C.J. van Oss, R.F. Giese, Z. Li, K. Murphy, J. Norris, M.K. Chaudhury, R.J. Good, Determination of contact angles and pore sizes of porous media by column and thin layer wicking, J. Adhes. Sci. Technol. 6 (1992) 413–428.
[59] R.J. Good, Contact angle, wetting and adhesion: a critical review, J. Adhes. Sci. Technol. 6 (1992) 1269–1302.
[60] H.Y. Erbil, Calculation of spreading pressure from contact angle data on polymer surfaces, Langmuir 10 (1994) 2006–2009.
[61] C. Ozcan, N. Hasirci, Evaluation of surface free energy for PMMA films, J. Appl. Polym. Sci. 108 (2008) 438–446.
[62] N. Erdogan, F. Erden, A.T. Astarlioglu, M. Ozdemir, S. Ozbay, G. Aygun, L. Ozyuzer, ITO/Au/ITO multilayer thin films on transparent polycarbonate with enhanced EMI shielding properties, Curr. Appl. Phys. 20 (2020) 489–497.
[63] S.R. Chalana, V.P. Mahadevan Pillai, Substrate dependent hierarchical structures of RF sputtered ZnS films, Appl. Surf. Sci. 440 (2018) 1181–1195.
[64] M.L. Plumer, J. van Ek, D. Weller, The Physics of Ultra-High-Density Magnetic Recording, Springer, Heidelberg, 2001.
[65] J. Karamdel, A. Hadi, C.F. Dee, B.Y. Majlis, Effects of substrate on surface morphology, crystallinity, and photoluminescence properties of sputtered ZnO nano films, Ionics 18 (2012) 203–207.
[66] O. Guellati, D. Bégin, F. Antoni, S. Moldovan, M. Guerioune, C. Pham-Huu, I. Janowska, CNTs' array growth using the floating catalyst-CVD method over different substrates and varying hydrogen supply, Mater. Sci. Eng. B. 231 (2018) 11–17.
[67] Y.S. Yoon, Y.K. Yoon, J.Y. Lee, S.S. Yom, Surface morphologies of $BaTiO_3$ thin films by atomic force microscopy, Jpn. J. Appl. Phys. 33 (1994) 4075–4079.
[68] X. Fang, C.L. Mak, J. Dai, K. Li, H. Ye, C.W. Leung, ITO/Au/ITO sandwich structure for near-infrared plasmonics, ACS Appl. Mater. Interfaces. 6 (2014) 15743–15752.
[69] K. Hong, K. Kim, S. Kim, I. Lee, H. Cho, S. Yoo, H.W. Choi, N.Y. Lee, Y.H. Tak, J. L. Lee, Optical properties of WO_3/Ag/WO_3 multilayer as transparent cathode in top-emitting organic light emitting diodes, J. Phys. Chem. C. 115 (2011) 3453–3459.
[70] C. Guillén, J. Herrero, Optical, electrical and structural characteristics of Al:ZnO thin films with various thicknesses deposited by DC sputtering at room temperature and annealed in air or vacuum, Vacuum 84 (2010) 924–929.
[71] C. Guillén, J. Herrero, Influence of oxygen in the deposition and annealing atmosphere on the characteristics of ITO thin films prepared by sputtering at room temperature, Vacuum 80 (2006) 615–620.
[72] H. Sahm, C. Charton, R. Thielsch, Oxidation behaviour of thin silver films deposited on plastic web characterized by spectroscopic ellipsometry (SE), Thin Solid Films 455–456 (2004) 819–823.
[73] Y. Suzuki, Y. Ojima, Y. Fukui, H. Fazyia, K. Sagisaka, Post-annealing temperature dependence of infrared absorption enhancement of polymer on evaporated silver films, Thin Solid Films 515 (2007) 3073–3078.
[74] D.R. Sahu, J.L. Huang, Design of ZnO/Ag/ZnO multilayer transparent conductive films, Mater. Sci. Eng. B. 130 (2006) 295–299.
[75] D.R. Sahu, C.Y. Chen, S.Y. Lin, J.L. Huang, Effect of substrate temperature and annealing treatment on the electrical and optical properties of silver-based multilayer coating electrodes, Thin Solid Films 515 (2006) 932–935.
[76] Y.S. Jung, Y.W. Choi, H.C. Lee, D.W. Lee, Effects of thermal treatment on the electrical and optical properties of silver-based indium tin oxide/metal/indium tin oxide structures, Thin Solid Films 440 (2003) 278–284.
[77] H.S. Roh, S.H. Cho, W.J. Lee, Study on the durability against heat in ITO/Ag-alloy/ITO transparent conductive multilayer system, Phys. Status Solidi Appl. Mater. Sci. 207 (2010) 1558–1562.
[78] A. Klöppel, W. Kriegseis, B.K. Meyer, A. Scharmann, C. Daube, J. Stollenwerk, J. Trube, Dependence of the electrical and optical behaviour of ITO-silver-ITO multilayers on the silver properties, Thin Solid Films 365 (2000) 139–146.
[79] S.J. Nadel, Durability of Ag based low-emissivity coatings, J. Vac. Sci. Technol. A. 5 (1987) 2709–2713.
[80] K. Koike, S. Fukuda, Multilayer transparent electrode consisting of silver alloy layer and metal oxide layers for organic luminescent electronic display device, J. Vac. Sci. Technol. A. 26 (2008) 444–454.
[81] E. Ando, M. Miyazaki, Moisture resistance of the low-emissivity coatings with a layer structure of Al-doped ZnO/Ag/Al-doped ZnO, Thin Solid Films 392 (2001) 289–293.
[82] J.Y. Lee, J.W. Yang, J.H. Chae, J.H. Park, J.I. Choi, H.J. Park, D. Kim, Dependence of intermediated noble metals on the optical and electrical properties of ITO/metal/ITO multilayers, Opt. Commun. 282 (2009) 2362–2366.
[83] J. Lewis, S. Grego, B. Chalamala, E. Vick, D. Temple, Highly flexible transparent electrodes for organic light-emitting diode-based displays, Appl. Phys. Lett. 85 (2004) 3450–3452.
[84] J.W. Seo, J.W. Park, K.S. Lim, S.J. Kang, Y.H. Hong, J.H. Yang, L. Fang, G.Y. Sung, H.K. Kim, Transparent flexible resistive random access memory fabricated at room temperature, Appl. Phys. Lett. 95 (2009), 133508.
[85] M. Sawada, M. Higuchi, S. Kondo, H. Saka, Characteristics of indium-tin-oxide/silver/indium-tin-oxide sandwich films and their application to simple-matrix liquid-crystal displays, Jpn. J. Appl. Phys. 40 (2001) 3332–3336.
[86] H.K. Park, J.W. Kang, S.I. Na, D.Y. Kim, H.K. Kim, Characteristics of indium-free GZO/Ag/GZO and AZO/Ag/AZO multilayer electrode grown by dual target DC sputtering at room temperature for low-cost organic photovoltaics, Sol. Energy Mater. Sol. Cells. 93 (2009) 1994–2002.
[87] T. Minami, T. Miyata, T. Yamamoto, Stability of transparent conducting oxide films for use at high temperatures, J. Vac. Sci. Technol. A. 17 (1999) 1822–1826.
[88] J. Montero, C. Guillén, J. Herrero, AZO/ATO double-layered transparent conducting electrode: A thermal stability study, Thin Solid Films. 519 (2011) 7564–7567.